IJE TRANSACTIONS A: Basics Vol. 37 No. 07, (July 2024) 1208-1220

International Journal of Engineering

Journal Homepage: www.ije.ir

Performance of Pile Group in Soils Prone to Liquefaction Affected by Far and Near Earthquakes

M. R. Gavadimoghaddam, N. Hadiani*, S. M. A. Sadreddini, A. H. Eqbali

Department of Civil Engineering, Islamshahr Branch, Islamic Azad University, Tehran, Iran

P A P E R I N F O

Paper history:
Received 07 August 2023
Received in revised form 16 December 2023
Accepted 30 December 2023

Keywords:
Liquefaction
Soil Liquefaction
Building Pile
System Dynamics
Numerical Modeling

A B S T R A C T

The aim of the current research is to investigate the pile group functions in liquefaction prone soil under the influence of far and near earthquakes and structural responses such as acceleration history, displacement and bending moments. The method of estimating the response spectrum of the building was used according to the distance, size, structural conditions and fault mechanism and measuring the response spectrum of a selected recorded or artificial earthquake. By using opensees software, Midas Gts, different modes of research were formed. In the selection of earthquake accelerometers for the far and near areas, Peer Seismography Center, Iran Accelerography Center and Road and Housing Research Center were used to select and modify the accelerometers. The results of the research showed that increasing the diameter of the pile reduces the possibility of liquefaction, so that by increasing the diameter of the pile from 0.5 m to 1 m, the possibility of liquefaction and collapse of the pile group decreases by about 33%. In addition, with an increase in the distance between the piles, the probability of liquefaction increases, so that the probability of liquefaction of the group of piles and its collapse increases by about 14% when the distance between the piles increases from 1.5 to 5 meters. Finally, using the results of numerical modeling and with coding software, a suitable model for the pile group against liquefaction was presented for earthquakes in the far and near domains.

***doi**: 10.5829/ije.2024.37.07a.01*

Graphical Abstract

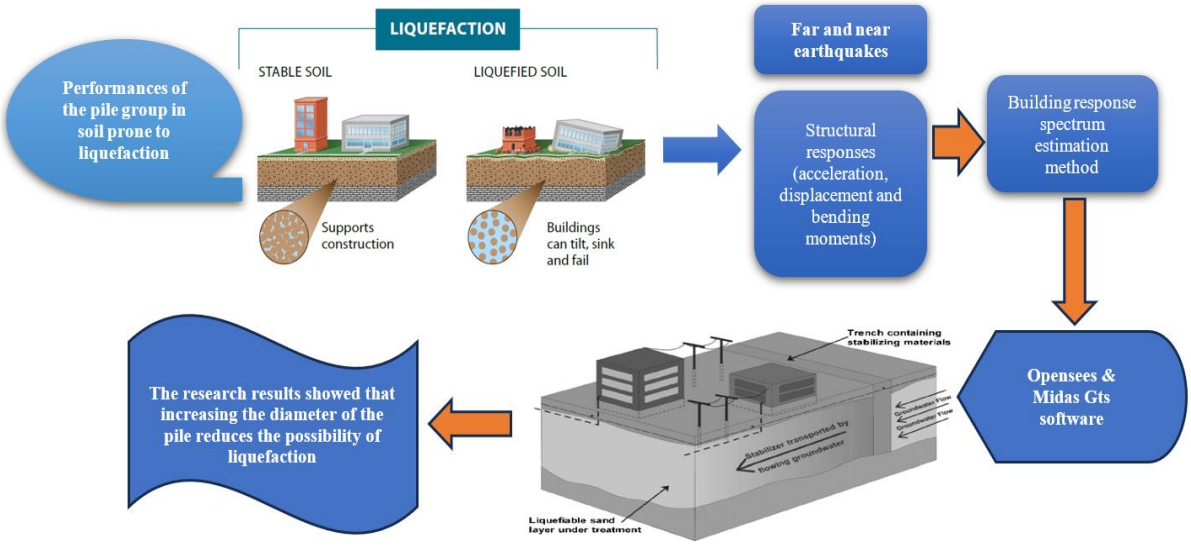

* Corresponding Author Institutional Email: n.hadiani@gmail.com (N Hadiani)

Please cite this article as: Gavadimoghaddam MR, Hadiani N., A Sadreddini SM, Eqbali AH. Performance of Pile Group in Soils Prone to Liquefaction Affected by Far and Near Earthquakes. International Journal of Engineering, Transactions A: Basics. 2024;37(07):1208-20.

1. INTRODUCTION

The damages caused by the earthquake may be directly attributed to the effects of earthquake or may be the indirect result of its direct damages. In addition, direct damages may be caused by the primary effects of shaking (namely, earthquakes and fault displacements) or secondary effects such as landslides and soil liquefaction, which themselves arise from the primary effects (1). Liquefaction is a term used to describe phenomena in which the production of excess pore water pressure leads to significant softening or weakening of soil deposits (2). This softening can be caused by dynamic loading or static loading. The phenomenon of changing the behavior of sand from solid state to liquid state was recognized in the first steps of expanding the knowledge of soil mechanics (3). Observing the destruction and failure of surface foundations due to liquefaction and lateral expansion in past earthquakes has revealed the need to fully understand the effects of this phenomenon on surface foundations. In such a way that the seismic response studies of foundations in liquefied soil are now one of the main topics of research in seismic geotechnical engineering. Significant research efforts have been made in this field over the past few years.

The review of past studies shows good information about parameters affecting liquefaction, but still there is a lack of a comprehensive parametric study considering earthquakes in the near area and the effects related to the type of faulting and extrawall and subwall effects. The lateral expansion caused by liquefaction has caused severe damage to many important structures during earthquakes (4). As a result, the evaluation of mass response to lateral expansion is an important step towards safe and resistant design against this destructive phenomenon (5). The purpose of the current research is to study the response of the group of piles that are exposed to lateral expansion caused by liquefaction, the responses of the structure such as the history of acceleration, displacement and bending moments should be investigated. In addition, the distribution of lateral soil pressure and movement patterns around the piles should be investigated and based on the results of the analysis of the responses of the pile group for different earthquake states (far field and near field), a suitable model for the design and arrangement of the pile group for different states should be made. According to the research conducted in non-flowing soils, the appropriate relative distance for arranging the piles is 3 to 5 times the diameter of the pile.

Fluidization has a significant effect on the dynamic response of the piles and increases the displacement of the pile compared to the non-fluidized state (6). Now, the question arises that in liquefied soils, can the same arrangement be used, or do other factors that result from the effect of liquefaction on the dynamic response of the pile group have an effect on the choice of arrangement? In this research, an attempt is made to answer this question by studying this problem with the help of numerical modeling with the finite element method, and based on that, the optimal distance in flowable soils for the pile group is obtained. In this research, the assumption of a continuous environment and the assumption of large deformations are used.

At first, for an earthquake record, parametric studies will be done on the distance between the piles. Considering the importance of earthquakes in the nearby area, the effect of these earthquakes on liquefaction will also be investigated. Earthquakes in the near-fault zone are characterized by a shock movement with a short duration and a long period, which exposes the structure to a large input energy at the beginning of the record (7). This pulsed motion is particularly common in the forward direction ("progressive directionality"), where the fault rupture propagates toward the structure at a speed close to that of the shear wave. The "permanent displacement effect" which is the result of the displacement of the residual earth due to the tectonic deformations related to the failure mechanism, is described by a one-way velocity pulse with a long amplitude and with a uniform step in the time history of the displacement (8). Another feature of these earthquakes is the "overwall effect" which is created due to the proximity of the buildings on the overwall to the fault plane compared to the buildings with the same distance on the downwall (9). Investigating this factor (underwall or extrawall effect) on the structure and if the structure is in the area of the extrawall or underwall, what acceleration will it receive and how will the response of the structure be in front of these accelerations. Another important feature is "vertical component effect". The reason for the importance of this characteristic is the greater ratio of the maximum vertical to horizontal acceleration of the earth in records near the fault compared to far from the fault. Considering the importance of knowing the characteristics of these earthquakes, the characteristics of earthquakes near the fault and far from the fault and the effect of these on the acceleration on the structure and the type of failure and the design mechanism of the pile group for each of the acceleration pulses and providing a suitable model and taking into account the effect of types. The fault movements and liquefaction conditions are from the Shama group's plan using parametric analysis in the field of finite elements and dynamic analysis, i.e. Midas and Opensees, which will be done using the outputs of these two softwares and checking, comparing and relating the results of these two softwares. The purpose of this research is to provide a suitable model of the pile group design against lateral expansion resulting from liquefaction for near and far earthquakes.

2. MATHEMATICAL MODEL

In short, the research steps are as follows. The first step provides an overview of earthquakes in far and near areas. In the next step, numerical modeling for different research situations is created using opensees, Midas Gts engineering software. The number of research models is based on the number of variables. Another research step covers the use of the specific constitutive model or liquefaction. In the selection of earthquake accelerometers for far and near areas, the Peer Seismography Center, the National Accelerography Center, and the Road and Housing Research Center are used to select and modify the accelerometers. Finally, a suitable model is presented for the pile group against liquefaction for far and near-field earthquakes using the results of numerical modeling and coding software. To check the effect of the overwall and underwall, the pile group is once modeled above the fault (the pile group on the side where the fault moves upwards) and again below the fault (the pile group on the side where the fault moves downwards). Then, the behavior of Shama group is investigated against earthquakes in far and near areas.

In this article, all the simulations were done in three stages using OpenSees software. After validating the numerical model using centrifuge test, analysis was done for different conditions. By comparing the numerical results with the centrifuge test, it can be concluded that the use of P-Y curves with different degradation factors in flowable sand brings reasonable results. In addition, the non-parallel surface layer plays a key role in ground displacement, especially in sloping terrain.

2. 1. The Record Selection Method Selecting a number of earthquake records is the first step of incremental dynamic analysis. Here, a set of 40 three-component ground motion records (in three directions) without scale, each in the direction of the normal multiplication component, is used as earthquake excitation. This group of records has a large and almost constant variance around the average spectral values in different periods. The last feature ensures that earthquake records with different specification ranges are available for analysis and the aleatory ground motion uncertainty can be considered in situations where researchers are interested in evaluating the effect of ground motion variance on structural response estimation.

2. 2. Introduction of the UBCSAND Constitutive Model In this research, the UBCSAND constitutive model was used to investigate the behavior of liquefacted sand under dynamic loading. UBCSAND is a two-dimensional effective stress plasticity model that is used in advanced stress-deformation analysis of geotechnical structures (10-19). This model was developed to investigate the behavior of sandy soils with liquefaction potential under dynamic loading (e.g. sands and silty sands with a relative density of approximately less than 80%). In this model, the stress-shear behavior of the soil is forecasted using a hypothetical hyperbolic relationship and the volumetric strain of the soil skeleton with a flow rule that is a function of the instant stress ratio. This model can perform a fully-coupled analysis in which the mechanical calculations and water flow are considered simultaneously and parallelly. In the UBCSAND constitutive model, the elastic components of the soil response with shear modulus $\boldsymbol{G^e}$ and bulk modulus $\boldsymbol{B^e}$ are specified as follows:

$$G^e = K_G^e . P_a . (\frac{\sigma'}{P_a})^{n_e} \quad (1)$$

$$B^e = \alpha . G^e \quad (2)$$

where K_G^e is the shear modulus number that depends on the relative density and ranges from 500 for loose sand to 2000 for dense sand. P_a is the atmospheric pressure, σ' is the average all-round stress in the loading plane, n_e ranges from 0.4 to 0.6 and is almost equal to 0.5, and α refers to Poisson's ratio. Plastic strains are controlled by yield surface and flow rule. The yield surface is expressed by a radial line passing through the origin of the stress space as shown in the figure. For the first shear loading, the yield surface is controlled by the current stress state (point A in Figure 1). When the shear stress increases, the stress ratio ($\eta = \frac{\tau}{\sigma'}$) increases and causes the stress point to move to point B. τ and $\sigma'$are the effective shear and normal stresses in the maximum effective shear stress plane. The yield surface is moved to a new location that passes through point B and the origin, leading to the creation of shear and volumetric plastic strains. The development of shear plastic strain is obtained by $d\gamma^p = \frac{1}{G^p/\sigma'} . d\eta$ where G^p is the plastic shear modulus. Further, it is assumed that a hyperbolic relationship exists between η and G^pas follows:

$$\boldsymbol{G^p = G_p^i . (1 - \frac{\eta}{\eta_f} . R_f)^2} \quad (3)$$

where G_p^i is the plastic modulus at a low stress ratio. η_f is the ratio of stress and tension in rupture equal to $\sin \emptyset_f$where $\emptyset_f$ is the maximum friction angle. R_f is the rupture ratio which is used to fit the best hyperbolic relationship and avoid overpredicting the resistance during the rupture. R_f varies from 0.7 to 0.98 and decreases by increasing relative density (20, 21).

$d\varepsilon_v^p$ refers to the plastic volume strain development, and p represents the flow rule. Further, $d\gamma^p$ refers to the plastic shear strain development according to the following equation.

$$\boldsymbol{d\varepsilon_v^p = (\sin \emptyset_{cv} - \frac{\tau}{\sigma'}) d\gamma^p} \quad (4)$$

where $\emptyset_{cv}$is the constant volume friction angle or the phase transformation angle.

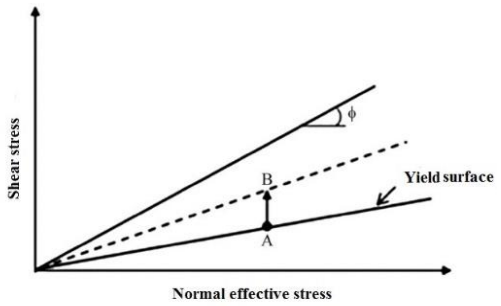

Figure 1. Yield surface in the UBCSAND model (10)

2. 3. Introduction of Moore-Coulomb's Constitutive Model The Mohr-Coulomb model is often used for granular materials, such as MIDAS GTS concrete. In this model, the stress-strain relationship is considered as a complete elastic paste. Figure 2 presents Mohr-Coulomb yield criterion based on assumption causes a logical solution in nonlinear analysis.

The Mohr-Coulomb failure criterion is determined according to the failure envelope based on the Mohr stress circles and $F_1(\sigma)$from laboratory tests. This criterion is a more general form of the Tresca criterion, in this way that the maximum shear stress is the yield criterion, but the maximum shear stress depends on the condition the compressive stresses are dependent. In other words, the following equation is true in the two-dimensional state:

$$|T| = F_1(\Sigma) \quad (5)$$

where τ is the maximum shear stress and σ is the compressive stress. F_1 is the function obtained from the test. The simplest form of function $F_1(\sigma)$, is a linear function. We can display this linear function as follows:

$$|T| = C - \Sigma \tan \Phi \quad (6)$$

where c and φ are obtained from experimental results. Physically, c is adhesion and φ is the angle of internal friction. This relationship was first presented by Coulomb and then independently by Mohr.

In the case that σ_1≥σ_2≥σ_3, using the principal stresses, the Mohr-Coulomb criterion is written as follows:

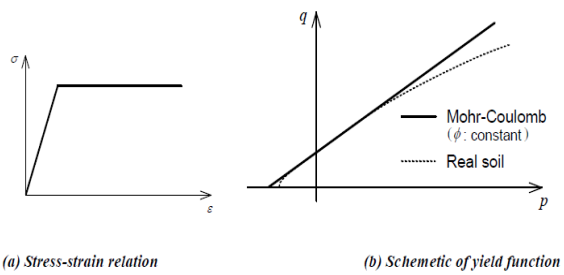

(a) Stress-strain relation *(b) Schemetic of yield function*

Figure 2. Mohr-Coulomb yield criterion (22)

$$\Sigma_1 \frac{(1-\sin\Phi)}{2c\cos\Phi} - \Sigma_3 \frac{(1+\sin\Phi)}{2c\cos\Phi} = 1 \quad (7)$$

The Mohr-Coulomb failure surface is an irregular hexagon in the 3D space of principal stresses. where the bisector is a straight line. Figure 3 shows the Moore-Coulomb fracture surface in the three-dimensional apparatus of principal stresses. The failure surface of a regular octagon is located on the π plane ($\sigma_1 + \sigma_2 + \sigma_3 = 0$).

$$\rho_{to} = \frac{2\sqrt{6}c\cos\varphi}{3+\sin\varphi} \quad (8)$$

$$\rho_{co} = \frac{2\sqrt{6}c\cos\varphi}{3-\sin\varphi} \quad (9)$$

$$\frac{\rho_{to}}{\rho_{co}} = \frac{3-\sin\varphi}{3+\sin\varphi} \quad (10)$$

The Mohr-Coulomb yield surface on π plane and bisector plane is shown in Figure 4.

2. 4. Specifications of Numerical Model in Midas Software In this research, a two-dimensional model was used based on the type of analysis and the time-consuming nature of the analysis. Figure 1 shows

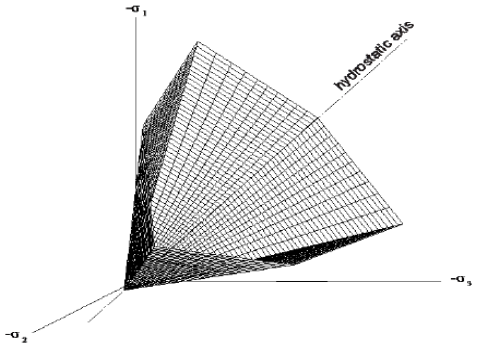

Figure 3. A view of the Moore-Coulomb fracture surface in the three-dimensional apparatus of principal stresses (6)

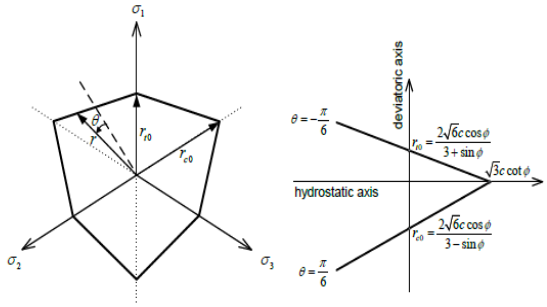

(a) Yield surface on π -plane *(b) Yield surface on meridian plane ($\theta = -\frac{\pi}{6}$)*

Figure 4. Mohr-Coulomb yield surface on π plane and bisector plane (12)

components in the numerical model. The model in the software includes three parts: Soil, pile, and foundation. The model consists of 4 layers of soil, respectively. The first layer is 2 meters thick, the second layer is liquefiable soil with a thickness of 5 meters, the third layer is 2 meters thick granular soil, and the last layer is a 15-meter thick weak rock. There is a foundation with a thickness of 1 meter and a length of 5 meters above the soil. Under the foundation, 4 piles with different distances and different lengths are modeled according to the type of analysis. Figure 5 shows the numerical model built in Midas.

2. 5. Boundary Conditions Elastic boundaries are needed in the boundaries due to the dynamic analysis of the model. For a better and more optimal performance of the process of applying the acceleration time history during seismic dynamic analysis, if boundaries are simultaneously elastic, the state with viscose, false, and intensified vibrations disappear and the model will be more closer to reality (23). The necessary tools are available in the Midas GTS software. In this regard, the supports are perpendicular to the plane with the spring capability of the bed itself. According to the following equation, they have damping coefficients to create a viscose mode. The equations for the coefficients of damping and damping are as follows:

$$k_{V0} = k_{h0} = \frac{1}{30} \cdot \alpha \cdot E_0 \quad (11)$$

It ranges from 1 to 4 according to the sample and laboratory conditions. The ground reaction coefficients (K_V, K_h) can be obtained by the following equation (in cm):

$$K_V = k_{V0} = \left(\frac{B_V}{30}\right)^{\frac{-3}{4}}, B_V = \sqrt{A_V} \quad (12)$$

Damping coefficients C_P, C_S are also calculated using Figure 6 as follows:

$$C_P = \rho \cdot A \cdot \sqrt{\frac{\lambda+2G}{\rho}} = W \cdot A \cdot \sqrt{\frac{\lambda+2G}{W\times 9.81}} = c_P \cdot A \quad (13)$$

$$C_S = \rho \cdot A \cdot \sqrt{\frac{G}{\rho}} = W \cdot A \cdot \sqrt{\frac{G}{W\times 9.81}} = c_S \cdot A \quad (14)$$

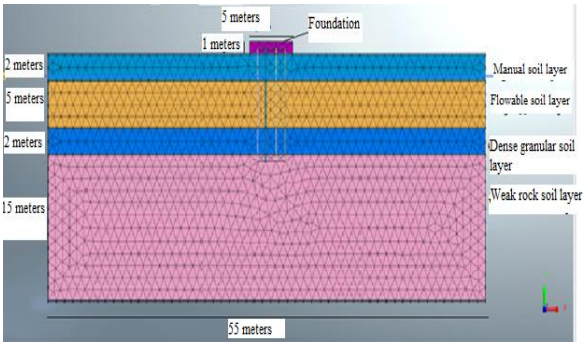

Figure 5. Numerical model built in Midas

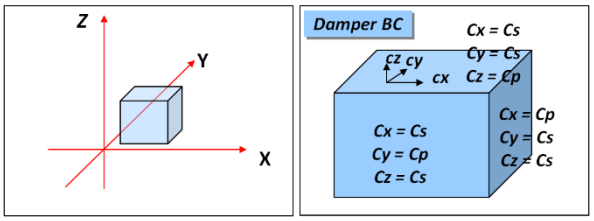

Figure 6. Components of the damping coefficient in the general coordinate system (10)

$$\lambda = \frac{\nu E}{(1+\nu)(1-2\nu)}, G = \frac{E}{2(1+\nu)} \quad (15)$$

The seismic risk estimation and design criteria for x, y, z directions are presented based on the acceleration results of artificial maps in the region, as well as the history of accelerations that are proposed as seismic design criteria. Design engineers should understand how loads are carried from the to piles and soil media so they can predict performance like settlement, bearing pressure enhancement, and borrowing capacity rate, as well as behavior like displacement and load sharing across (10). (Experimental Study of Lateral Loading on Piled Raft Foundations on Sandy Soil).Therefore, the acceleration history is selected based on this critical seismic profile in the software. It is worth noting that the vibration period is reduced to 10 seconds by ignoring the low-amplitude vibrations to shorten the analysis period or run the numerical model. In this way, the model is ready to be analyzed under the influence of the benchmark acceleration history in the main coordinate directions. It should be noted that a simple static analysis is necessary for the mesh control. Further, there is a need for eigenvalues and natural vibration periods of different modes of the model, which is also obtained by taking an Eigenvalue analysis for dynamic analysis settings. Additionally, the Rayleigh damping value of 0.05 is used in the dynamic analysis (11).

3. NUMERICAL MODELING AND ANALYSIS RESULTS

This research introduces a set of records of earthquakes in the near field with a pulse caused by the progressive directionality in the time history of the speed of earth's movement. Assuming the problem that the location of accelerograms is on the bedrock, 10 accelerograms (5 near-field accelerograms and 5 far-field accelerograms), recorded on hard rock, are used for analysis. Table 1 presents the specifications of these accelerometers.

3. 1. Analysis Parameters In this research, 4 parameters were subjected to sensitivity analysis. The analysis parameters included the pile length, pile diameter, pile distance, and pile load. For sensitivity

TABLE 1. Records of earthquakes in the near area

Earthquake	Year	Station	Tp	PGV	Mw
San Fernando	1971	Pacoima Dam	1.6	28	6.6
Coyote Lake	1979	Gilroy Array	1.2	4	5.7
Morgan Hill	1984	Coyote Lake Dam	1	27	6.2
Cape Mendocino	1992	Petrolia	3	47	7
Northridge -01	1994	Pacoima Dam	0.5	34	6.7

analysis, each of the four parameters are studied three times. Table 2 presents the number of far-field analyses. The analysis parameters of the pile groupn are summarized in Table 3.

3. 2. Geotechnical Specifications of the Model

The Moore-Coulomb model was used for non-liquefiable layers, and the UBCSAND constitutive model was used for liquefiable soil. The following tables present the parameters for each layer.

The model used in the free response analysis of the soil in this article is a finite element model in which the soil layers are modeled by the FourNodeQuadUP element and in two modes of pressure-dependent materials and pressure-independent materials with multifaceted yield surfaces. These materials can be used in two-dimensional and three-dimensional elements. Explanations related to these two items are provided below.

nDMaterial PressureDependMultiYield $tag $nd $rho $refShearModul $refBulkModul $frictionAng $peakShearStra $refPress $pressDependCoe $PTAng $contrac $dilat1 $dilat2 $liquefac1 $liquefac2 $liquefac3 where in:

$tag number of material used

$nd the number of dimensions that can be 2 for plane strain and 3 for three-dimensional analysis.

$rho is the saturated mass density of the substance

$refShearModul soil shear module

$refBulkModul is the bulk modulus of the soil obtained from equation 25-4

$frictionAng internal soil friction angle

$peakShearStra octahedral shear strain where the maximum shear strength occurred and from the relation

$$E_b = \frac{2}{3}G\frac{1+\nu}{1-2\nu} \quad (16)$$

$$\gamma = \frac{2}{3}\left[\left(\varepsilon_{xx}-\varepsilon_{yy}\right)^2+\left(\varepsilon_{yy}-\varepsilon_{zz}\right)^2+\left(\varepsilon_{xx}-\varepsilon_{zz}\right)^2+6\varepsilon_{xy}^2+6\varepsilon_{yz}^2+6\varepsilon_{xz}^2\right]^{1/2} \quad (17)$$

$refPress Confinement average pressure where , and are defined.

$pressDependCoe is a non-negative coefficient that represents the G and B variables as a function of the effective confinement coefficient, which is based on the following relationship.

$$G = G_r\left(\frac{P'}{P_r}\right)^d \qquad B = B_r\left(\frac{P'}{P_r}\right)^d \quad (18)$$

$PTAng phase change angle in degrees

$contrac is a non-negative coefficient that represents the volume reduction or pore water pressure production.

$dilat1, 2 coefficients that are used as indicators of volume increase or expansion.

$liquefac1 parameters that control the liquefaction mechanism.

3. 3. Calibration of Materials

The Morcoulomb pattern behavior was used to calibrate the model materials, using the three-axis experiemntasl results of

TABLE 2. Records of earthquakes in far area

Earthquake	Year	Station	Tp	PGV	Mw
San Fernando	1971	Lake Hughes	-	10	6.6
San Fernando	1971	Santa Anita Dam	-	11	6.6
Manjil Iran	1990	Abbar	-	29	7.4
Taiwan SMARTI	1986	SMART1 E02	-	36.7	7.3
Nahanni	1985	Site 1	-	15	6.76

TABLE 3. Parameters used for non-liquefacted and liquefacted materials

	(kN/m^2)	(kN/m^3)	Sat (kN/m^2)	C (kN/m^2)	Φ	K(cm/s)	v	Ψ
EMBANKEMENT	4000	18	20	15	25	0.1	0.35	1
WEATHER ROCK	1000000	20	51	35	33	0.1	0.3	7
SOFT ROCK	900000	24	25	150	37	0.01	0.01	7

Material	E(kN/m^2)	Y(kN/m^3)	Y Sat (kN/m^2)	P0 (kN/m^2)	ELASTIC SHEAR MODULUS	ELASTIC SHEAR MODULUS
LIQUFACTIOM LAYER	60000	20	21	100	1069	0.5

the calibration. To calibrate, an axially symmetric two-dimensional model was created in the software with all experiemntasl conditions for performing three-axis tests on model materials. In this model, a triaxial cylinder is used with a diameter of 15 cm, a height of 30 cm, with 48 nodes, and 33 elements. Figure 6 shows the axial symmetry section of the triaxial test in MIDAS GTS. The calibration curves of materials and product materials in the CD test under 6 kg/cm^2 are shown in Figures 7 and 8, respectively.

3. 4. Length Change Results This section examines the results of changes in pore water pressure ratio, as well as the liquefaction criterion ratio for different acceleration maps. Figures 9 and 10 show the acceleration maps of 1 and 5, respectively.

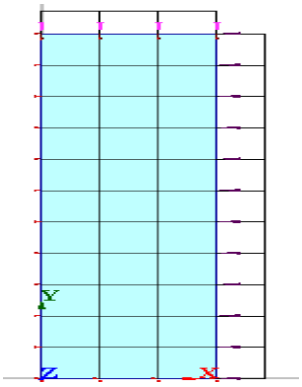

Figure 6. Triaxial geometry pattern in MIDAS GTS

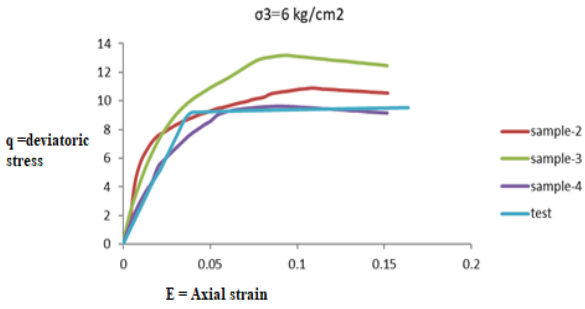

Figure 7. Calibration of materials in the CD test under 6 kg/cm^2 all-round stress

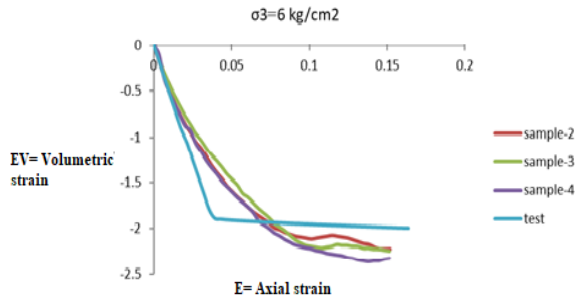

Figure 8. Calibrated product of materials in CD test under 6kg/cm^2 all-round stress

3. 4. 1. Bore Water Pressure Results With changes in the length of the pile (5, 8 and 10) meters for 5 distant earthquake records, the pore water pressure decreases with an increase in the pile length. Further, the pressure changes start from the 4th second onwards for most of the acceleration maps. The rate of changes decreases with increasing the candle length.

3. 4. 2. The Results of the Ratio of Shear to Vertical Stress (Liquefaction Criterion) With changes in the pile length (5, 8, and 10 meters) for 5 distant earthquake records, the ratio of the maximum stress decreases with an increase in the pile length. Further, the stress changes start from the 4th second onwards for most acceleration maps. Additionally, the rate of changes decreases with an increase in the pile length. Based on the diagrams for all deflection maps, the probability that liquefaction will occur is close to zero for a pile with a length of 10 meters. The acceleration map 1 normalized maximum stress ratio is shown in Figure 11.

3. 5. The Results of Changing the Candle Diameter This section examines the results of changes in the pore water pressure ratio and the liquefaction criterion ratio

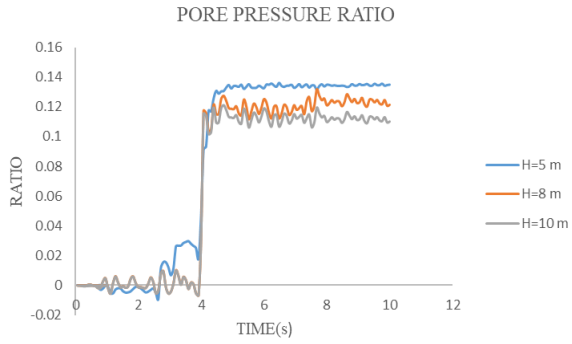

Figure 9. Acceleration map 1

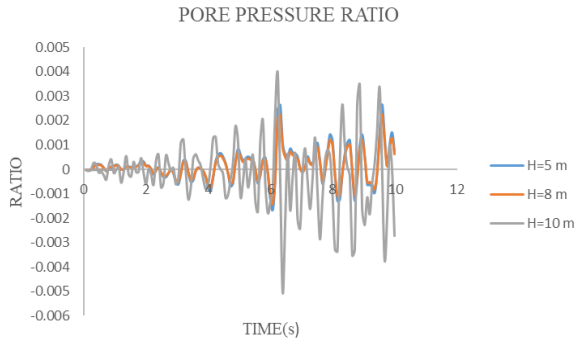

Figure 10. Acceleration map 5

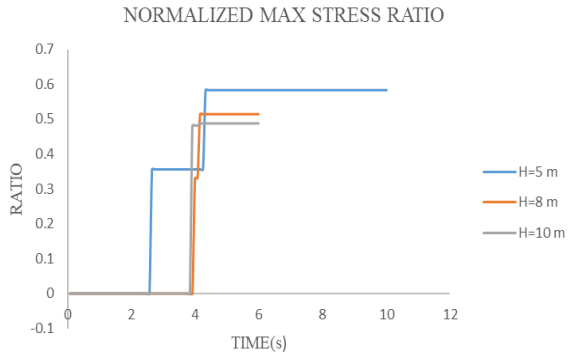

Figure 11. Acceleration map 1

for the acceleration of different mappings with changes in the pile diameter.

3. 5. 1. Results of Pore Water Pressure With the changes in pile diameter (0.5, 0.8, and 1 meters) for 5 earthquake records in the far area, an increase in the pile diameter raises the pore water pressure, as well as the pressure changes from 4th second onwards for most of the acceleration maps. Additionally, the rate of change increases with an increase in candle diameter. An increase in the ratio of pore water pressure is due to the greater confinement of soil between the piles with an increase in the pile diameter. The acceleration map 1 pore pressure ratio is shown in Figure 12.

3. 5. 2. The Results of the Ratio of Shear to Vertical Stress (Liquefaction Criterion) With the changes in pile diameter (0.5, 0.8 and 1) meters for 5 remote area earthquake records, it can be seen that with the increase in pile diameter, the maximum stress ratio has a decreasing trend, and also the stress changes from the 4th second onwards for most of the acceleration maps start Also, the rate of change decreases with the increase of the diameter of the pile. Also, by checking the graphs for all acceleration maps, it can be seen that the probability of liquefaction is less for piles with a length of 10 meters.

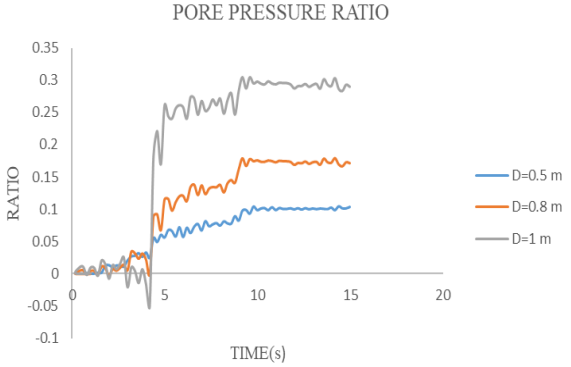

Figure 12. Acceleration map 1

For the acceleration mapping number 4, diameter 0.8 has given a lower stress ratio than the pile with a diameter of 1 meter. This inconsistency in the results is due to the convergence operator of the analysis, which was difficult for the navigation map number 4 due to the acceleration of the analysis convergence mapping, and this contradiction is due to the difference in the convergence of the analysis. The acceleration map 1 normalized maximum stress ratio for 0.5, 0.8 and 1m is shown in Figure 13.

3. 6. The Results of Changing the Candle Distance This section examines the results of changes in pore water pressure ratio, as well as the liquefaction criterion ratios for different acceleration mappings under the effect of pile distance changes.

3. 6. 1. Bore Water Pressure Results With the changes in pile distance (1.5, 2.5, and 5 meters) for 5 distant earthquake records, an increase in pile distance decreases the pore water pressure. Further, the pressure changes from 4th second onwards for most of the acceleration maps. The rate of change is constant with increasing candle distance. The reduction of the pore water pressure ratio is due to the reduction of soil confinement between the piles by increasing the pile distance. The acceleration maps 1 and 5 pore pressure ratio for 1.5, 2.5 and 5m are shown in Figures 14 and 15, respectively.

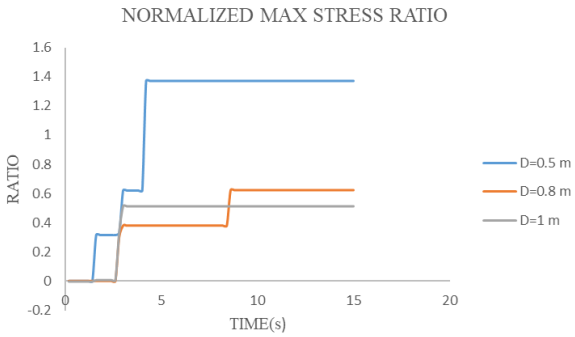

Figure 13. Acceleration map 1

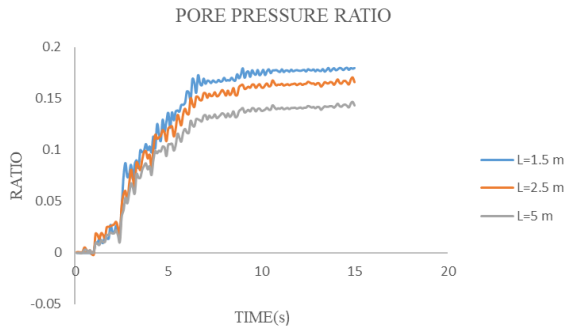

Figure 14. Acceleration map 1

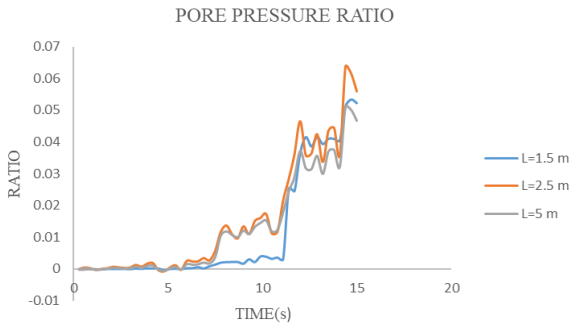

Figure 15. Acceleration map 5

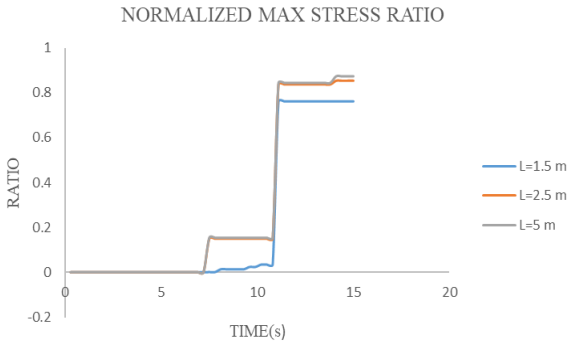

Figure 17. Acceleration map 5

3. 6. 2. The Results of the Ratio of Shear to Vertical Stress (Liquefaction Criterion) Based on changes in pile spacing (1.5, 2.5, and 5 meters) for 5 earthquake records in the far area, an increase in pile spacing raised the ratio of the maximum stress, and also the stress changes from the 4th second onwards for most of the acceleration maps. Further, the rate of changes with increasing pile distance is almost constant. Based on the diagrams for all acceleration maps, short pile distance reduces the probability of liquefaction for almost 5 earthquakes, but the rate of decrease in the probability of liquefaction is lower with increasing distance from 2 to 5 meters, indicating that increasing the pile distance beyond a certain limit has no effect on liquefaction. The acceleration maps 1 and 5 normalized maximum stress ratio are shown in Figures 16 and 17, respectively.

3. 7. Results of Changing the Pile Load This section presents the results of changes in pore water pressure ratio, as well as liquefaction criterion ratio for different acceleration mappings under the effect of load changes on the piles.

3. 7. 1. Results of Bore Water Pressure Based on changes in the load on the pile foundation (1, 5, and 10 tons) for 5 records of far-field earthquakes, an increase in the pile load decreases the pore water pressure, as well as the pressure changes from the 4th second onwards for most of the acceleration maps. Additionally, the rate of change is constant with an increase in entering the candle. The reduction of the pore water pressure ratio is due to the increase in effective soil stress between the piles with an increase in the pile load. The acceleration map 5 pore pressure ratio is shown in Figures 18.

3. 7. 2. The Results of the Ratio of Shear to Vertical Stress (Liquefaction Criterion) Based on changes in the load on the pile foundation (1, 5, and 10 tons) for 5 earthquake records in the far area, an increase in the pile load decreases the ratio of the maximum stress, and the stress changes start from the 4th second onwards for most of the acceleration maps. Addiotnally, the rate of change increases with an increase in the pile load. Based on the graphs for all acceleration maps, an increase in the pile load reduces the probability of liquefaction for almost 5 earthquakes, and these changes increase with the load. The acceleration map 1 normalized maximum stress ratio is shown in Figure 19.

3. 8. Incremental Dynamic Analysis The incremental dynamic analysis method is a non-linear dynamic analysis that can determine the level of damage by the earthquake intensity. In this method, the scaling of the acceleration maps of past earthquakes is used in such a way that it covers the structure behavior from a linear

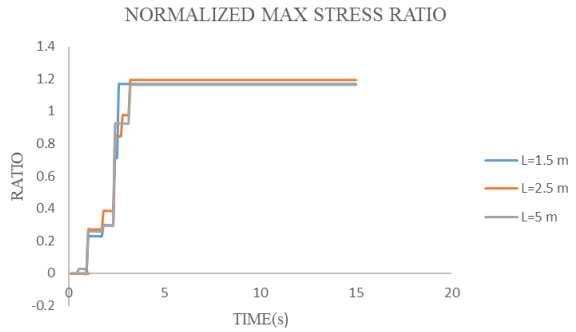

Figure 16. Acceleration map 1

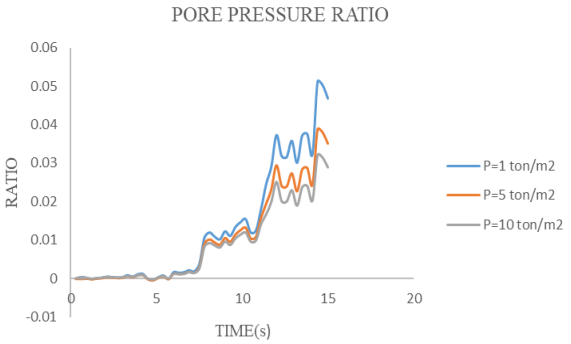

Figure 18. Acceleration map 5

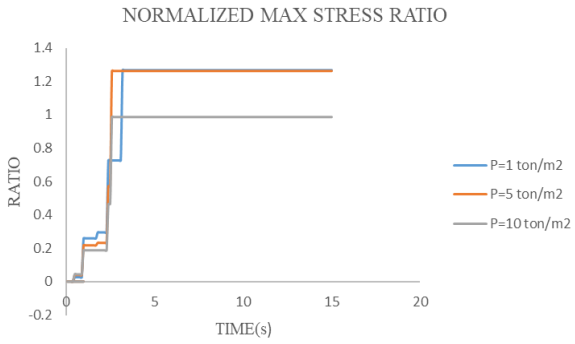

Figure 19. Acceleration map 1

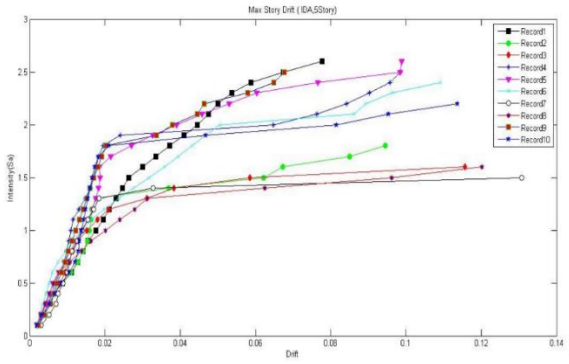

Figure 20. A set of IDA curves for a five-story structure

elastic to a collapse stage of the structure. In this method, which is also developed to consider the effect of inherent uncertainty in earthquakes, the seismic response of structures is evaluated to take into account the uncertainty of frequency and spectral shape of earthquakes. Further, an appropriate number of earthquake records should be used. Each earthquake record is scaled in such a way to cover a suitable range of earthquake intensities and structure behavior from elastic limit to failure (24, 25).

To perform the analysis, first, the seismic intensity parameter is considered, for example, the maximum ground acceleration or spectral acceleration corresponding to the first mode of the structure, from a very small value for the occurrence of elastic behavior in the structural model under dynamic analysis to a certain level of seismic intensity to achieve the desired failure limit, with an appropriate algorithm. Each time, this scale factor is applied to the earthquake record, and the structure under the influence of that record becomes a dynamic time history analysis. At the end of each analysis stage, the level of damage intensity corresponding to the earthquake intensity level, in which the analysis is performed, is recorded. Finally, under each scaled record, a response curve is obtained against the intensity that is referred as the IDA single record curve.

The structure behavior under an earthquake record cannot be generalized for all records because the result is not general and cannot be considered as the general behavior of the structure under all conditions at different times and earthquakes. Several single-record curves are needed to conduct probabilistic and statistical studies to achieve the correct result of the structure's behavior; hence, this operation is performed for all desired records, and the resulting single record curves are all drawn in a seismic intensity-damage intensity coordinate system, called IDA curves. Figure 20 shows the IDA curves for a five-story structure.

3. 8. 1. Incremental Dynamic Analysis (IDA) Results for Different Pile Diameters Even though the structure's behavior under an earthquake record is important but cannot be generalized for all records because the result does not have a general state and cannot be considered the general behavior of the structure under all conditions at different times and earthquakes, in other words, for evaluating the seismic behavior of the structure. Several single curves are necessary to achieve the correct result of behavior. Based on IDA curves, there are 15 records for the candles in the figures below**.** Based on the curves, all stages of pile group behavior under earthquake can be fully observed from elastic to collapse limit, and general instability. At the beginning of all curves, there is an elastic region as a straight line and a part of the IDA curve as a common section of all curves. After this area, the nonlinear behavior is visible in the curves when the curve leaves the a straight line. Further, a decrease in hardness or its increase show the nonlinear behavior. Therefore, this set of curves can get a general view of soil and pile behavior from full elastic limit to full failure. A comparison of the behavior of piles at different diameters and on the same type of ground incates that an increase in the diameter of piles leads to the entry of the pile group into the nonlinear region and a higher capacity. Figure 21 illustrates the IDA diagram for a pile in 1 m diameter.

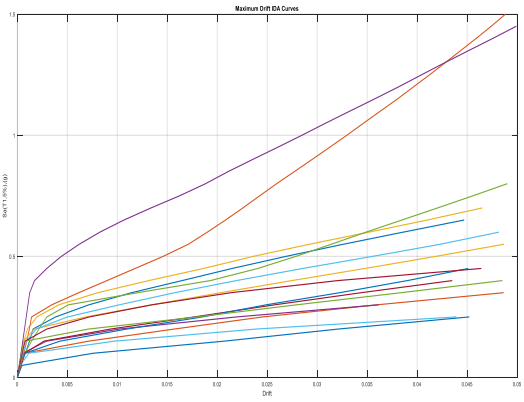

Figure 21. IDA diagram for a pile in a diameter of 1 m

3. 8. 2. The probability of Liquefaction for Different Pile Diameters under Far-field Records

Fragility curves are used to extract the probability of limit states from the output of IDA. To draw these curves, IM values corresponding to the occurrence of the desired limit state are arranged in descending order for all records. Then, the probability of occurrence of the limit state in the pile is calculated using the sorted values, and its curve is drawn against IM. Based on the curve, an increase in the diameter of piles at a fixed level of seismic intensity decreases the probability of collapse or lack of a performance level. The fragility curves for different diameters is shown in Figure 22.

Based on the results, an increase in pile diameter decreases the probability of liquefaction so that the probability of pile group liquefaction and collapse decreases by about 33% when the diameter of piles increases from 0.5 to 1 meters. It is also significant. When the diameter increases from 0.5 to 0.8 meters, the probability of liquefaction decreases by about 12%. Table 4 summarized numerical analysis of liquefaction probability.

3. 8. 3. Results of IDA for Different Pile Distances

The IDA method greatly depends on the acceleration map and the desired structure. Therefore, the same models sometimes show different behaviors under the influence of different acceleration maps. The occurrence of a specific and linear region in seismic intensities is common among all IDA curves. This linear behavior ends with the appearance of the first submission in the candlestick. The slope of this linear area is an indicator of elastic stiffness of the structure and is different under the effects of different records on the structure. After crossing the linear region, the behavior of the IDA curve is different and varied. After the first yield in the members in some cases, a sharp drop in the curve occurs and the graph quickly moves towards larger values of the failure criterion. In other cases, the curve becomes steeper due to hardening. In some cases, the curve oscillates around its initial slope in a way that expresses successive hardening and softening. This phenomenon occurs due to the irregular nature of the record so that the acceleration or the force resulting from the earthquake causes damage at a certain time of the acceleration map. Based on the occurrence of yielding in some members at other times, this acceleration decreases so much and turns the curve into a lower failure criterion or even reverses the direction of the curve. Comparing the behavior of piles at different distances (3d, 5d, 10d) equivalent to 1.5, 2.5, and 5 meters on the same type of ground indicates that an increase in distance between the piles leads to the quick entry of the pile group into the nonlinear region at a lower capacity. The IDA diagram for 5d distance is shown in Figure 23.

3. 8. 4. The Probability of Liquefaction Occurrence for Different Pile Distances under Far Field Records

The fragility curves are used to extract the probability of occurrence of limit states from the output of IDA. Based on the curves, an increase in the distance of piles at a fixed level of seismic intensity increases the probability of collapse or failure to meet the performance level. Figure 24 shows analytical analysis of the fragility curve at different distances.

The results indicate that the possibility of liquefaction increases with an increase in the pile distance so that the probability of liquefaction and collapse of the pile group increases by about 14% when the pile distance increases from 1.5 to 5 meters. The probability of liquefaction increases by 7% when the distance increases from 1.5 to 2.5 meters.

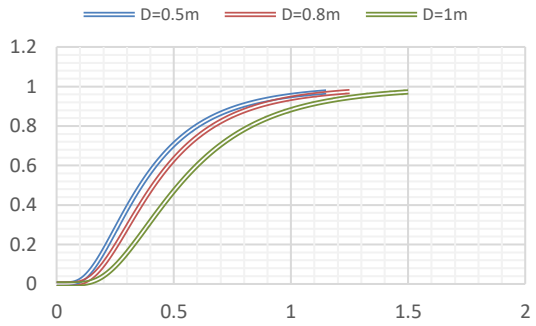

Figure 22. Fragility curve for different diameters

TABLE 4. Numerical study of liquefaction probability

	D=0.5m	D=0.8m	D=1m
Sa(T1,g)	0.5	0.5	0.5
Probability%	70	62	47

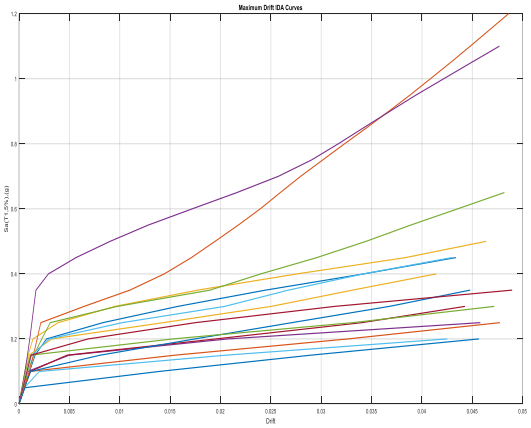

Figure 23. IDA diagram for 5d distance

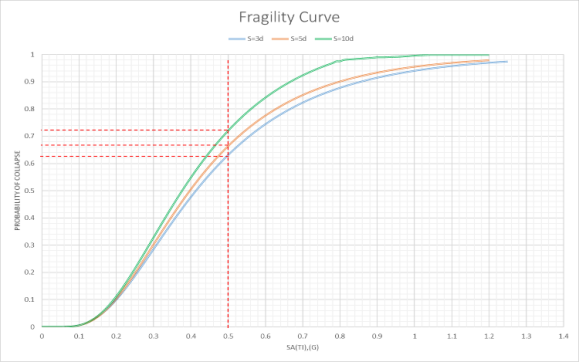

Figure 24. Analytical investigation of the fragility curve at different distances

4. CONCLUSION

With changes in the length of the pile (5, 8 and 10) meters for 5 distant earthquake records, it can be seen that with the increase in the length of the pile, the pore water pressure has a decreasing trend, and also the pressure changes start from the 4th second onwards for most of the acceleration maps. The rate of change decreases with increasing candle length. Also, the stress changes start from the 4th second onwards for most of the acceleration maps, and the rate of change decreases with the increase in the length of the pile. In addition, by checking the graphs for all the swing maps, it can be seen that for a pile with a length of 10 meters, the probability that Liquefaction occurs close to zero. By checking the graphs for all acceleration maps, it can be seen that the probability of liquefaction is less for piles with a length of 10 meters. For the acceleration mapping number 4, diameter 0.8 has given a lower stress ratio than the pile with a diameter of 1 meter. This inconsistency in the results is due to the convergence of the analysis, which for the number 4 floating map, according to the type of acceleration, the convergence of the analysis was difficult, and this contradiction is due to the difference in the convergence of the analysis. Also, the pressure changes from the 5th second onwards for most of the acceleration maps. Likewise, the rate of change decreases with increasing candle length. The rate of change decreases with the increase in the length of the pile. Also, by checking the graphs for all deflections, it can be seen that for a pile with a length of 10 meters, the probability that liquefaction will occur is very low. Comparing the behavior of piles with different diameters and on the same type of ground, it can be said that by increasing the diameter of the piles, the pile group enters the nonlinear region later and has more capacity. As the diameter of the pile increases, the possibility of liquefaction decreases, so that the possibility of liquefaction and collapse of the pile group decreases by about 33% when the diameter of the piles increases from 0.5 to 1 meter, which is a significant number. Also, when the diameter increases from 0.5 meters to 0.8 meters, the probability of liquefaction decreases by about 12%. Comparing the behavior of piles with different distances (3d, 5d, 10d) is equivalent to (1.5, 2.5 and 5) meters on the same type of ground, it can be said that by increasing the distance between the piles, the pile group enters the nonlinear region earlier and has a lower capacity.

5. REFERENCES

1. Zomorodian R, Soltani F, Sivandi-Pour A, Noroozinejad Farsangi E. Effect of foundation flexibility on the seismic performance of a high-rise structure under far-field and near-field earthquakes. International Journal of Engineering, Transactions A: Basics. 2021;34(7):1611-22. 10.5829/ije.2021.34.07a.06
2. Kamrani Moghaddam P, Manafpour A. Effects of Far-and Near-Field Multiple Earthquakes on the RC SDOF Fragility Curves Using Different First Shock Scaling Methods. International Journal of Engineering. 2018;31(9):1505-13.
3. Pan R, Xu C, Jia K, Dou P, Kamran I. Large-scale shaking table test and three-dimensional numerical simulation research on earthquake seismic failure response of laterally spreading site-pile group-superstructure system. Bulletin of Earthquake Engineering. 2023;21(10):4789-819. https://doi.org/10.1007/s10518-023-01713-y
4. Sahare A, Ueda K, Uzuoka R. Influence of the sloping ground conditions and the subsequent shaking events on the pile group response subjected to kinematic interactions for a liquefiable sloping ground. Soil Dynamics and Earthquake Engineering. 2022;152:107036. https://doi.org/10.1016/j.soildyn.2021.107036
5. Chandiwala A, Vasanwala S. Experimental study of lateral loading on piled raft foundations on sandy soil. International Journal of Engineering. 2023;36(1):28-34. 10.5829/ije.2023.36.01a.04
6. Mohammadizadeh M, Bostani M, Farkat E, Mohammadizadeh N. Soil-Structure Interaction Effect on seismic response of Low-and mid-rise steel moment frames equipped with Pall friction damper. Amirkabir Journal of Civil Engineering. 2023;55(7):1337-62. 10.22060/ceej.2023.20880.7559
7. Motamed R, Towhata I, Honda T, Tabata K, Abe A. Pile group response to liquefaction-induced lateral spreading: E-Defense large shake table test. Soil Dynamics and Earthquake Engineering. 2013;51:35-46. https://doi.org/10.1016/j.soildyn.2013.04.007
8. Loli M, Knappett JA, Brown MJ, Anastasopoulos I, Gazetas G. Centrifuge modeling of rocking-isolated inelastic RC bridge piers. Earthquake engineering & structural dynamics. 2014;43(15):2341-59. https://doi.org/10.1002/eqe.2451
9. Haeri SM, Rajabigol M, Salaripour S, Kavand A, Sayyaf H, Afzalsoltani S, et al. Effects of physical modeling boundary conditions on the responses of 3× 3 pile groups to liquefaction induced lateral spreading Bulletin of Earthquake Engineering. 2023;21(5):2469-502. https://doi.org/10.1016/j.soildyn.2023.107915
10. Li W, Chen Y, Stuedlein AW, Liu H, Zhang X, Yang Y. Performance of X-shaped and circular pile-improved ground subject to liquefaction-induced lateral spreading. Soil Dynamics and Earthquake Engineering. 2018;109:273-81. https://doi.org/10.1016/j.soildyn.2018.03.022
11. Casagrande A, editor The determination of the pre-consolidation load and its practical significance. Proc 1st Int Conf Soil Mech; 1936.

12. Casagrande A. Characteristics of cohesionless soils affecting the stability of slopes and earth fills. J Boston Society of Civil Engineers. 1936;23(1):13-32.
13. Wang Y, Orense RP. Numerical analysis of seismic performance of inclined piles in liquefiable sands. Soil Dynamics and Earthquake Engineering. 2020;139:106274. https://doi.org/10.1016/j.soildyn.2020.106274
14. Wang X, Ye A, Shang Y, Zhou L. Shake-table investigation of scoured RC pile-group-supported bridges in liquefiable and nonliquefiable soils. Earthquake Engineering & Structural Dynamics. 2019;48(11):1217-37. https://doi.org/10.1002/eqe.3186
15. Jia K, Xu C, El Naggar MH, Zhang X, Du X, Dou P, et al. Large-scale shake table testing of pile group-bridge model in inclined liquefiable soils with overlying crusts. Soil Dynamics and Earthquake Engineering. 2022;163:107555. https://doi.org/10.1016/j.soildyn.2022.107555
16. Li W, Stuedlein AW, Chen Y, Liu H, Cheng Z. Response of pile groups with X and circular cross-sections subject to lateral spreading: 3D numerical simulations. Soil Dynamics and Earthquake Engineering. 2019;126:105774. https://doi.org/10.1016/j.soildyn.2019.105774
17. Ghorbani A, Hasanzadehshooiili H, Somti Foumani MA, Medzvieckas J, Kliukas R. Liquefaction Potential of Saturated Sand Reinforced by Cement-Grouted Micropiles: An Evolutionary Approach Based on Shaking Table Tests. Materials. 2023;16(6):2194. 10.3390/ma16062194
18. Lombardi D, Bhattacharya S. Evaluation of seismic performance of pile-supported models in liquefiable soils. Earthquake Engineering & Structural Dynamics. 2016;45(6):1019-38. 10.1002/eqe.2716
19. Wang Y, Orense RP. Numerical Investigation of Inclined Piles under Liquefaction-Induced Lateral Spreading. Geotechnics. 2023;3(2):320-46. https://doi.org/10.3390/geotechnics3020019
20. Knappett J, Madabhushi S. Liquefaction-induced settlement of pile groups in liquefiable and laterally spreading soils. Journal of geotechnical and geoenvironmental engineering. 2008;134(11):1609-18. https://doi.org/10.1061/(ASCE)1090-0241(2008)134:11(1609)
21. Mao W, Liu B, Rasouli R, Aoyama S, Towhata I. Performance of piles with different configurations subjected to slope deformation induced by seismic liquefaction. Engineering geology. 2019;263:105355. https://doi.org/10.1016/j.enggeo.2019.105355
22. Saha P, Horikoshi K, Takahashi A. Performance of sheet pile to mitigate liquefaction-induced lateral spreading of loose soil layer under the embankment. Soil Dynamics and Earthquake Engineering. 2020;139:106410. https://doi.org/10.1016/j.soildyn.2020.106410
23. Moghaddam PK, Manafpour A. Effects of Far-and Near-Field Multiple Earthquakes on the RC Single Degree of Freedom Fragility Curves Using Different First Shock Scaling Methods. International Journal of Engineering, Transactions C: Aspects. 2018;31(9):1505-13. 10.5829/ije.2018.31.09c.05
24. Iraji A. Evaluating Finn-Byrne Model in Liquefaction Analysis of Quay Wall and Cantilevered Retaining Wall Models. International Journal of Engineering, Transactions C: Aspects. 2023;36(6):1075-91. 10.5829/ije.2023.36.06c.06
25. Razavi SA, Siahpolo N. A New Optimal Correlation for Behavior factor of EBFs under Near-fault Earthquakes using Artificial Intelligence Models. International Journal of Advanced Structural Engineering. 2022;12(2):631-45. 10.1007/ijase.2022.698628

Persian Abstract

چکیده

هدف از پژوهش حاضر بررسی عملکردهای گروه شمع در خاک‌مستعد روانگرایی تحت تأثیر زلزله‌های حوزه دور و نزدیک و پاسخ‌های سازه از قبیل تاریخچه شتاب، جابجایی و گشتاورهای خمشی می باشد. از روش تخمین طیف پاسخ ساختگاه با توجه به فاصله، بزرگا، شرایط ساختگاهی و مکانیزم گسلش و مقیاس کردن طیف پاسخ یک زلزله منتخب ثبت شده یا مصنوعی، متناسب با آن استفاده گردید. با استفاده از نرم‌افزارهای opensees، Midas Gts حالات مختلف تحقیق شکل گرفت. در انتخاب شتاب‌نگاشت‌های زلزله برای حوزه دور و حوزه نزدیک از مرکز لرزه‌نگاری Peer، مرکز شتاب‌نگاری کشور و مرکز تحقیقات راه و مسکن برای انتخاب و اصلاح شتاب‌نگاشت‌ها استفاده شد. نتایج تحقیق نشان داد که افزایش قطر شمع احتمال روان‌گرایی را کاهش می‌دهد به‌گونه‌ای که با افزایش قطر شمع از ۰.۵ متر به ۱ متر، احتمال روان‌گرایی و فروپاشی گروه شمع حدود ۳۳ درصد کاهش می‌یابد. علاوه بر این، با افزایش فاصله شمع‌ها، احتمال روان‌گرایی افزایش می‌یابد به طوری که احتمال روان‌گرایی گروه شمع‌ها و فروپاشی آن با افزایش فاصله شمع‌ها از ۱.۵ به ۵ متر، حدود ١٤ درصد افزایش می‌یابد.در آخر با استفاده از نتایج حاصله از مدل‌سازی عددی و با نرم‌افزارهای کد نویسی الگویی مناسب برای گروه شمع در برابر روانگرایی برای زلزله‌های حوزه دور و حوزه نزدیک ارائه گردید.